Imaging the model through wave equations

Esteban Díaz, Satyan Singh, Roel Snieder, and Paul Sava

ABSTRACT

Marchenko two-way wavefields are able to reproduce complex wave phenomena that includes primaries, internal multiples and surface-related multiples. The wavefield contains reflections and information from the true model, but it is obtained by propagating with the kinematics of a background velocity model. We design an inverse problem in which we find a model that explains the scattering phenomena present in the wavefield. The two-way nature of the Marchenko wavefields allows us to insert them into the homogeneous wave equation and obtain images that are indicative of subsurface model parameters. Unlike conventional imaging methods, where the image is indicative of the interfaces in the subsurface, our method inverts for the properties throughout the subsurface. Our tests show that we can invert for images indicative of the true model even when the background velocity model is smooth. Furthermore, we are able to image properties from the true model that are not part of the inputs used to generate the wavefield.

Key words: inversion, wave equation, multiples

1 INTRODUCTION

Seismic imaging methods aim to estimate the Earth's reflectivity, i.e., a map of the interfaces that scatter the propagating wavefields. However, a seismic image does not only have structural information, but also dynamic properties that contain important information about the subsurface parameters (Etgen et al., 2009). Over the years, despite great advances in seismic exploration technology, the underlying imaging mechanism (the imaging condition) has remained similar to the one proposed by Claerbout (1971). The imaging condition simply states that reflectivity exists where the incident and scattered wavefields coincide in space and time. The amplitude is then given by the deconvolution or correlation of the incoming and outgoing fields.

The wavefield reconstruction step is where many advances occurred in recent years. The source and receiver wavefields can be extrapolated with integral formulations as in Kirchhoff migration (Schneider, 1978), one-way equations as in wave equation migration (WEM) (Gazdag, 1978; Gazdag and Sguazzero, 1984), or two-way equations as in reverse time migration (RTM) (Baysal et al., 1983; Whitmore, 1983; McMechan, 1983). The complexity of the velocity model and the geologic structure dictates which method is better suited. However, the three outlined families of methods share a basic assumption: the single-scattering (Born) approximation. Hence, the multiple-scattered waves present in the data are imaged in the wrong position. Therefore, the multiples are usually eliminated from the data as a pre-processing step (Verschuur et al., 1992; Weglein et al., 1997; Guitton, 2005; Lin and Herrmann, 2013) or from the migrated gathers as a post-imaging step (Sava and Guitton, 2005; Wang et al., 2010; Weibull and Arntsen, 2013).

In order to consider imaging beyond Born, several authors (Guitton, 2002; Grion et al., 2007; Verschuur and Berkhout, 2011; Whitmore et al., 2010; Wong et al., 2015) propose ideas for adapting more conventional technologies to handle multiples (surface-related in most cases). The adaptation requires prior separation of primaries and surface-related multiples. The primaries can then be used for imaging as an areal source for the down-going source wavefield, which correlates at the reflector position with the back propagated multiples. These approaches require an independent migration for each additional order of the multiple one seeks to incorporate into the seismic image.

Rose (2002a,b) proposes an inverse scattering approach based on focusing and time reversal which retrieves a function that focuses at an arbitrary point in an unknown 1D medium. This approach is extended to 2D and introduced to the geophysical community by Broggini and Snieder (2012). Their method yields the correct Green's function and properly handles primaries and internal multiples given a background velocity model with the appropriate kinematics. The Marchenko modeling framework (Broggini and Snieder, 2012; Behura et al., 2014; Wapenaar et al., 2014b; Singh et al., 2015a) solves for focusing functions that are used to compute the total Green's function, which can be decomposed into up- and down-going components. This framework is also applica-

ble to surface-related multiples (Singh et al., 2015a,b). The Marchenko modeling framework possesses interesting characteristics and differences with respect to the conventional propagators mentioned earlier: (1) it solves for the up- and down-going Green's functions in one step (as opposed to two independent propagation problems), (2) the up- and down-going Green's functions add-up to the total Green's function (whereas the conventional source and receiver wavefields do not), and (3) it naturally handles all scattering orders present in the data (as opposed to Born-modeling).

In this paper, we use the total Green's function instead of the individual up- or down-going components (or source and receiver wavefields) for obtaining an image of the model (instead of the reflectivity). When using the individual components of the wavefield, one usually applies an imaging principle similar to the one formulated by Claerbout (1971) for a reflectivity image. Instead, we use the total Green's functions together with relations given by the wave equation to obtain images sensitive to other subsurface properties like density or impedance. This paper is organized as follows: first we review the requirements and fundamentals for wave propagation with the Marchenko methodology, then we show how to obtain the subsurface properties from the wavefield; finally, we show synthetic examples where we invert for the velocity model and density images.

2 MARCHENKO IMAGING

In this section, we review the Marchenko framework outlined in Singh et al. (2015a) for the Green's function retrieval with pressure-normalized fields. Here we outline the modeling equations with the objective of highlighting the technical requirements for application of the framework. We refer the readers to Wapenaar et al. (2014b) and Singh et al. (2015a) for specific details about the derivation for flux- and pressure-normalized Marchenko frameworks, respectively.

2.1 Understanding the inputs for Marchenko

Let $R(\mathbf{x}_s, \mathbf{x}_r, t)$ be the pressure normalized response of a medium for sources $\mathbf{x}_s$ and receivers $\mathbf{x}_r$ located at $z = 0$. Note that R contains primaries, internal multiples, and surface-related multiples. Given this reflection response, the Marchenko framework retrieves the Green's function from a virtual source located at an arbitrary location $\mathbf{x}$ inside the medium (Singh et al., 2015a). The process relies on the computation of focusing solutions that, when injected at the surface, produce a concentration of energy (a focus) at time $t = 0$ at location $\mathbf{x}$. In order to retrieve such focusing solutions, one must inject the time-reversed inverse of the transmission response $T_d(\mathbf{x}, \mathbf{x}_r, t)$ from the point of interest to the surface. In practice, the direct arrival in the background medium approximates the inverse of the transmission response (Singh et al., 2015a).

2.2 Modeling

The Marchenko framework involves convolutions and correlations between the reflection response R, the focusing functions, and the transmission response T_d through an iterative process. Hence, the reflection response must be deconvolved with the source signature to avoid multiple convolutions with the source function.

The total wavefield $G(\mathbf{x}, \mathbf{x}_s, \omega)$ is the sum of its one-way components:

$$G(\mathbf{x}, \mathbf{x}_s, \omega) = G^+(\mathbf{x}, \mathbf{x}_s, \omega) + G^-(\mathbf{x}, \mathbf{x}_s, \omega), \quad (1)$$

and the up-going (G^-) and down-going (G^+) components are obtained through convolution and correlations of the reflection response R with the focusing functions f_1^+ and f_1^- (Singh et al., 2015a):

$$G^-(\mathbf{x}, \mathbf{x}_r, \omega) = -f_1^-(\mathbf{x}_r, \mathbf{x}, \omega) + \quad (2)$$
$$\sum_{\mathbf{x}_s} f_1^+(\mathbf{x}_s, \mathbf{x}, \omega)\, R(\mathbf{x}_r, \mathbf{x}_s, \omega) - r f_1^-(\mathbf{x}_s, \mathbf{x}, \omega)\, R(\mathbf{x}_r, \mathbf{x}_s, \omega),$$
$$G^+(\mathbf{x}, \mathbf{x}_r, \omega) = +f_1^+(\mathbf{x}_r, \mathbf{x}, \omega)^* - \quad (3)$$
$$\sum_{\mathbf{x}_s} f_1^-(\mathbf{x}_s, \mathbf{x}, \omega)^*\, R(\mathbf{x}_r, \mathbf{x}_s, \omega) - r f_1^+(\mathbf{x}_s, \mathbf{x}, \omega)\, R(\mathbf{x}_r, \mathbf{x}_s, \omega),$$

where r is the reflection coefficient at the free surface and * denotes complex conjugation. The individual components of the Green's function G satisfy the one-way reciprocity theorems shown by Wapenaar et al. (2014a), and the sum of its components satisfies the wave equation

$$\rho \nabla \cdot \left(\frac{1}{\rho} \nabla G \right) + \frac{\omega^2}{c^2} G = -j\omega\rho\delta(\mathbf{x} - \mathbf{x}_s). \quad (4)$$

The focusing functions are computed using the iterative framework described in Singh et al. (2015a).

3 IMAGING MODEL PARAMETERS

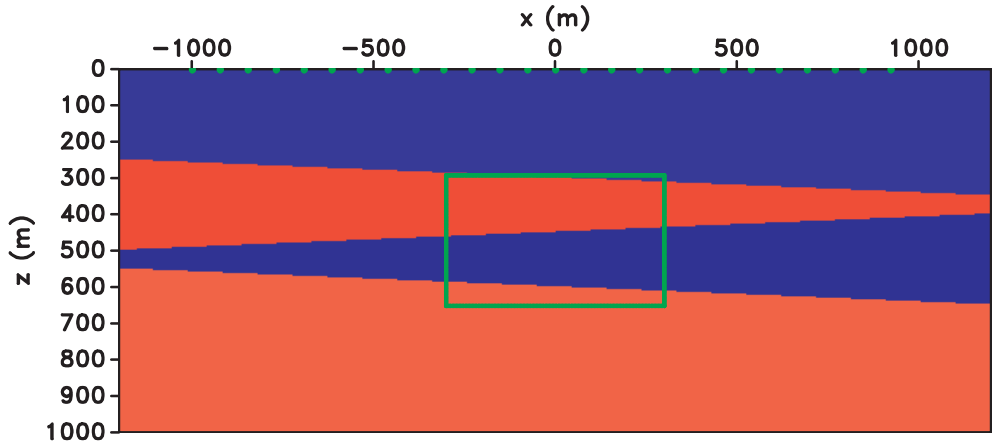
We use the total Green's function G to retrieve model parameters, like density and velocity, present in the wave equation and consider the modeling process in the previous section. The Marchenko modeling framework (Behura et al., 2014; Wapenaar et al., 2014b; Singh et al., 2015a) satisfies the acoustic wave equation; hence, we can use the retrieved wavefields as an input to the wave equation and solve for specific model parameters. A similar idea have been successfully implemented in the medical community for finding elastic parameters of human tissues (Manduca et al., 2001). Here we show an inversion framework for acoustic parameters.

3.1 Constant velocity acoustics

Consider the constant density homogeneous wave equation

$$s^2 \frac{\partial^2 u}{\partial t^2} - \nabla^2 u = 0, \quad (5)$$

where $s^2(\mathbf{x})$ is the slowness squared and $u(\mathbf{x}_s, \mathbf{x}, t)$ the Marchenko wavefield generated from the source location $\mathbf{x}_s$.



(a)

Figure 1. Variable velocity model: the points in the surface denote source locations and the highlighted box denotes the area in which the Marchenko wavefield is retrieved.

Note that the wavefield can be obtained inside the medium away from the source location $\mathbf{x}_s$ where the homogeneous equation is satisfied.

In order to solve for the unknown field $s^2(\mathbf{x})$, we set up a least-squares linear inverse problem based on the objective function

$$J(s^2) = \left|\left| s^2 \frac{\partial^2 u}{\partial t^2} - \nabla^2 u \right|\right|_2^2, \tag{6}$$

which has the formal solution:

$$s^2(\mathbf{x}) = \frac{\sum_{t,\mathbf{x}_s} \frac{\partial^2 u(\mathbf{x}_s,\mathbf{x},t)}{\partial t^2} \nabla^2 u(\mathbf{x}_s,\mathbf{x},t)}{\sum_{t,\mathbf{x}_s} \left(\frac{\partial^2 u(\mathbf{x}_s,\mathbf{x},t)}{\partial t^2}\right)^2}. \tag{7}$$

This expression closely resembles the least squares solution for the deconvolution imaging condition (Claerbout, 1971; Guitton et al., 2007). Here, instead of correlating the source and receiver wavefields, we correlate the laplacian of the total wavefield with its second time derivative.

The kinematics embedded in the Marchenko wavefield u are driven by the first arrival information $T_d(\mathbf{x}_s,\mathbf{x},t)$, which is computed using a background velocity model. The inversion procedure outlined in equation 6 utilizes the geometric attributes of the wavefield; therefore, the wave equation is satisfied for the same background velocity model used for computing the transmission response $T_d(\mathbf{x}_s,\mathbf{x},t)$.

3.2 Variable density acoustics

For a variable density field into the wave equation, the Marchenko wavefield u satisfies

$$\frac{s^2}{\rho}\frac{\partial^2 u}{\partial t^2} - \nabla\cdot\left(\frac{1}{\rho}\nabla u\right) = 0. \tag{8}$$

The relation of the wavefield $u(\mathbf{x}_s,\mathbf{x},t)$ to the model parameters slowness squared s^2 and density $\rho(\mathbf{x})$ is not as trivial as in the previous case. This problem does not have a direct least squares solution. Considering that the kinematics are controlled by the model used as input to compute T_d, we can focus our attention on the density model ρ. It is important to realize that using only the homogeneous wave equation (for pressure), one cannot retrieve the magnitude of the density field because it scales all the terms in the equation. However, one should be able to retrieve the relative changes in the density field. Similarly to the constant density case, we set an inverse problem with the following objective function:

$$J\left(\frac{1}{\rho}\right) = \left|\left| \frac{s^2}{\rho}\frac{\partial^2 u}{\partial t^2} - \nabla\cdot\left(\frac{1}{\rho}\nabla u\right)\right|\right|_2^2. \tag{9}$$

Numerically, the problem is implemented as follows:

$$J(m) = ||\mathbf{D_t} m + \mathbf{D}\mathbf{G_u} m||_2^2 = ||L(m)||_2^2, \tag{10}$$

where $\mathbf{D_t} = diag\{s^2(\mathbf{x})\frac{\partial^2 u(\mathbf{x}_s,\mathbf{x},t)}{\partial t^2}\}$, $\mathbf{G_u}$ is a block diagonal matrix that contains the gradient of u, and $\mathbf{D}$ is the divergence matrix.

The gradient with respect to the buoyancy $m = 1/\rho$ is given by

$$\nabla_m J = \mathbf{D_t}^\top L(m) + \mathbf{G_u}^\top \mathbf{D}^\top L(m), \tag{11}$$

where $^\top$ denotes adjoint. Once the gradient is defined, the model is updated iteratively using a non-linear solver.

3.3 Pressure and particle velocity relations

Another option for retrieving an image of the buoyancy is to use the relations between pressure fields and particle velocity. The Marchenko framework described in Singh et al. (2016) allows for the reconstruction of pressure u and the z component of the particle velocity v_z fields. Hence, we can find the model that best matches the acoustodynamics relation (given by the first-order linear relations given by Hooke's laws):

$$\frac{\partial V_z}{\partial t} = -\frac{1}{\rho}\frac{\partial u}{\partial z}. \tag{12}$$

From this system we can setup a linear inverse problem with the following objective function:

$$J(m) = \left|\left| \frac{\partial V_z}{\partial t} + m \frac{\partial u}{\partial z} \right|\right|_2^2, \tag{13}$$

which has the following solution:

$$m = -\frac{\sum_{t,\mathbf{x}_s} \frac{\partial V_z}{\partial t}(\mathbf{x}, \mathbf{x}_s, t) \frac{\partial u}{\partial z}(\mathbf{x}, \mathbf{x}_s, t)}{\sum_{t,\mathbf{x}_s} \left(\frac{\partial u}{\partial z}(\mathbf{x}, \mathbf{x}_s, t)\right)^2}. \tag{14}$$

The approaches presented here are not unique and, one could try for instance, to re-parametrize the wave equation in terms of acoustic impedance or other suitable combination. However, the strategy should fall into one of the presented methods. With a wrong background velocity model, it would not be possible to decouple the effect of model contrasts from the original model. Hence, it could be convenient to use impedance as the parameter that explains the reflections in the retrieved Marchenko wavefield.

4 EXAMPLES

We test the imaging procedure described in the preceding section for two cases: constant and variable density. For each case, we test the sensitivity to the background velocity model and compute acoustic data with a free surface boundary condition. In order to record both pressure and particle velocity data, we use the coupled acoustodynamics system of equations used in Thorbecke and Draganov (2011).

To retrieve the Marchenko wavefields, we place 500 sources and receivers at $z = 0$m in the range $x = [-1000, +1000]$m (Figure 1). The input transmission data $T_d(\mathbf{x}, \mathbf{x}_s, t)$ is computed using an eikonal solver to obtain the (model-dependent) travel-times $t_d(\mathbf{x}, \mathbf{x}_s)$ followed by a convolution with a Ricker wavelet with a peak of 40Hz:

$$T_d(\mathbf{x}, \mathbf{x}_s, t) = \delta\left(t - t_d\left(\mathbf{x}, \mathbf{x}_s\right)\right) * w(t). \tag{15}$$

The Ricker wavelet is the source function in this example, but in a real case scenario one must obtain a suitable source function from the data themselves.

Figure 1 shows the velocity model and the highlighted box depicts the area where the Marchenko wavefields are retrieved. The dots in the surface indicate the source locations used for the imaging process (a subset of the sources present in the data). The model consists of four layers of alternating velocity.

Figure 2(a) shows the background model inside the imaging box, which in this case is exact. The background model is used for computing the first arrivals (from the surface to the box locations). Figure 2(b) shows the retrieved velocity model (using equation 7), which converges to the true model in Figure 2(a). Figure 2(c) shows a wavefield snapshot at $t = 0.6$s for a source at $\mathbf{x}_s = (0, 0)$m. The retrieved Marchenko wavefield is the main input for the inversion. This result shows that the input wavefields do satisfy the homogeneous wave equation since the retrieved model converges to the input model used to create the data.

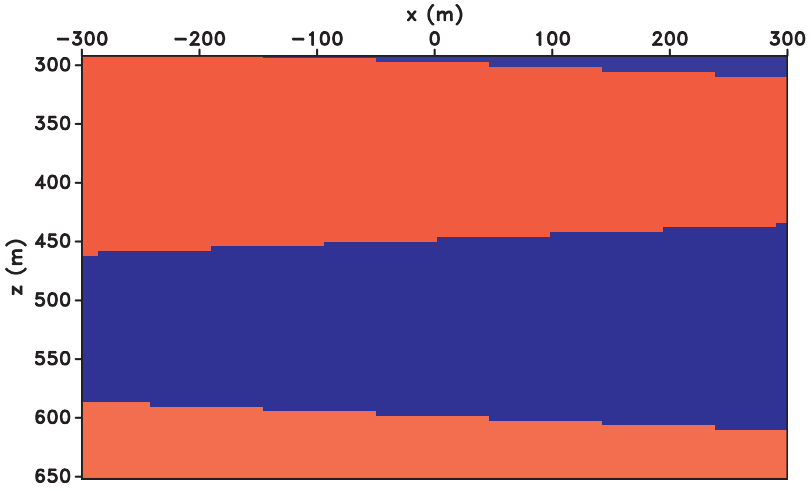
Figure 3(a) depicts a smooth version of the true velocity used as the background model. The Marchenko wavefields show propagating waves, with the corresponding reflections, even if the background velocity model is smooth. One could say that the retrieved wavefield are an expression of the true wavefield with the kinematics of the background model. Figure 3(b) is the inverted velocity model using the same procedure discussed above. Note that the inverted model still converges to the background model. This confirms that the kinematics of the retrieved wavefield are dominated by the background model, but the reflections present in the wavefield are due to the discontinuities of the original model. Figure 3(c) is the wavefield snapshot at the same time and location as in Figure 2(c) for the Marchenko wavefield propagated in the new background model which shows the reflections from the original model propagate with the kinematics of the background velocity.

4.1 Variable density model

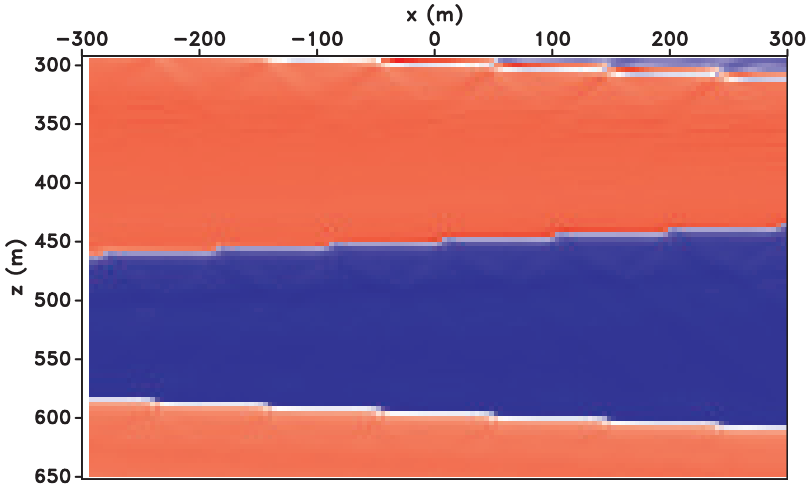
The model parameters for the variable density experiment are shown in Figures 4(a)-4(b). The density model contains two layers and its interface is decoupled from those in the velocity model. The model is designed in this fashion to see if the method is able to decouple the velocity from the density in the inversion. Since the kinematics of the wavefield converge to those of the background model, we focus our attention on the independent parameter, which is density in this case. Figure 5(a) shows the background model inside the box (the true model), whereas Figure 5(b) shows the inverted density model. The velocity interfaces leak into the inverted model, but the density layer and interface are well-imaged. Note that the density model is not an input for the computation of the wavefield shown in Figure 3(c) and yet the inverted image clearly delineates the density layer. In this example, we use the relation between pressure and particle velocity fields (equation 14) to compute the density image.

Figure 6(a) shows a smooth version of the true model used as background velocity field, and Figure 6(b) depicts the inverted density model. The density layer is clearly imaged despite the smooth background velocity model. The velocity interfaces again leak into the inverted model; interestingly, the background velocity model does not contain any interface (in a similar way as a conventional migrated image works) and yet the velocity interfaces from the original (true) model are imaged. One of the input wavefields for the inversion is shown in Figure 6(c). The wavefield propagates in the smooth background model (compare this with the snapshot in Figure 6(c)) and yet presents all the reflections from the true model.

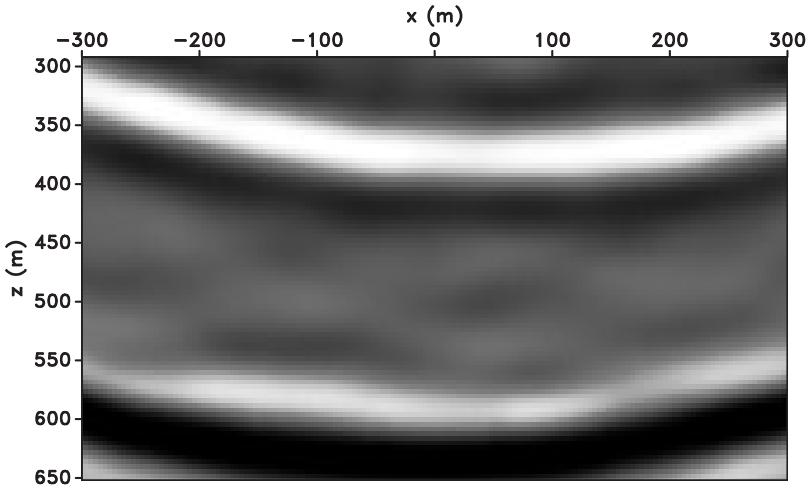
Figure 7 is a density inversion from the pressure field (equation 10). This type of inversion is more unconstrained (we have half the data). Also, by only using the pressure field, there is an ambiguity with the magnitude of the density model because many different density models can yield the same wavefield. The model is clearly imaged with this method, as the density layers are visible and there is only a hint from the velocity interface leaking into the inverted model. This ap-



(a)



(b)



(c)

Figure 2. Velocity retrieval: (a) is the (exact) background model used for computing the transmission response T_d, (b) is the retrieved velocity model, and (c) is a snapshot of the wavefield $G(\mathbf{x}, \mathbf{x}_s = (0,0), t = 0.6s)$

proach is a valid alternative if we only have the pressure data as input, instead of the pressure and particle velocity data needed for the previous variable density examples.

5 CONCLUSIONS

We present a framework to obtain images of acoustic model parameters that are different from reflectivity. Our method relies on two-way wavefields computed with Marchenko modeling. The wavefields are used with the wave equation together with the background velocity to find the model that explains, in a least-squares sense, the homogeneous wave equation. We show different options one could use depending on which type of data are available. One can exploit the relations between pressure and particle velocity and invert for the density model, or use an iterative approach if pressure is the only available data. Our tests show that it is possible to find an image representing the true model even when the background model is smooth. Our method is able to image the properties within the subsurface instead of the properties contrasts as it is done with conventional images.

6 ACKNOWLEDGMENTS

We thank the sponsors of the Center for Wave Phenomena, whose support made this research possible. The reproducible numeric examples in this paper use the Madagascar open-source software package (Fomel et al., 2013) freely available from http://www.ahay.org.

REFERENCES

Baysal, E., D. D. Kosloff, and J. W. C. Sherwood, 1983, Reverse time migration: Geophysics, **48**, 1514–1524.

Behura, J., K. Wapenaar, and R. Snieder, 2014, Autofocus imaging: Image reconstruction based on inverse scattering theory: Geophysics, **79**, A19–A26.

Broggini, F., and R. Snieder, 2012, Connection of scattering principles: a visual and mathematical tour: European Journal of Physics, **33**, 593.

Claerbout, J. F., 1971, Toward a unified theory of reflector mapping: Geophysics, **36**, 467–481.

Etgen, J., S. Gray, and Y. Zhang, 2009, An overview of depth imaging in exploration geophysics: Geophysics, **74**, WCA5–WCA17.

Fomel, S., P. Sava, I. Vlad, Y. Liu, and V. Bashkardin, 2013, Madagascar: open-source software project for multidimensional data analysis and reproducible computational experiments: Journal of Open Research Software, **1**, e8.

Gazdag, J., 1978, Wave equation migration with the phase-shift method: Geophysics, **43**, 1342–1351.

Gazdag, J., and P. Sguazzero, 1984, Migration of seismic data by phase shift plus interpolation: Geophysics, **49**, 124–131.

Grion, S., R. Exley, M. Manin, X. Miao, A. Pica, Y. Wang, P. Granger, and S. Ronen, 2007, Mirror imaging of obs data: first break, **25**.

Guitton, A., 2002, Shotprofile migration of multiple reflections: SEG Technical Program Expanded Abstracts 2002, 1296–1299.

———, 2005, Multiple attenuation in complex geology with a pattern-based approach: Geophysics, **70**, V97–V107.

Guitton, A., A. Valenciano, D. Bevc, and J. Claerbout, 2007, Smoothing imaging condition for shot-profile migration: Geophysics, **72**, S149–S154.

Lin, T. T. Y., and F. J. Herrmann, 2013, Robust estimation of primaries by sparse inversion via one-norm minimization: Geophysics, **78**, R133–R150.

Manduca, A., T. Oliphant, M. Dresner, J. Mahowald, S. Kruse, E. Amromin, J. Felmlee, J. Greenleaf, and R. Ehman, 2001, Magnetic resonance elastography: Non-invasive mapping of tissue elasticity: Medical Image Analysis, **5**, 237 – 254.

McMechan, G. A., 1983, Migration by extrapolation of time-dependent boundary values: Geophysical Prospecting, **31**, 413–420.

Rose, J., 2002a, Time reversal, focusing and exact inverse scattering, *in* Imaging of Complex Media with Acoustic and Seismic Waves: Springer Berlin Heidelberg, volume **84** *of* Topics in Applied Physics, 97–106.

Rose, J. H., 2002b, 'single-sided' autofocusing of sound in layered materials: Inverse Problems, **18**, 1923.

Sava, P., and A. Guitton, 2005, Multiple attenuation in the image space: Geophysics, **70**, V10–V20.

Schneider, W. A., 1978, Integral formulation for migration in two and three dimensions: Geophysics, **43**, 49–76.

Singh, S., R. Snieder, J. Behura, J. van der Neut, K. Wapenaar, and E. Slob, 2015a, Marchenko imaging: Imaging with primaries, internal multiples, and free-surface multiples: Geophysics, **80**, S165–S174.

Singh, S., R. Snieder, J. van der Neut, J. Thorbecke, E. Slob, and K. Wapenaar, 2015b, Incorporating free-surface multiples in marchenko imaging: SEG Technical Program Expanded Abstracts 2015, 4328–4333.

———, 2016, Accounting for free-surface multiples in marchenko imaging: submitted.

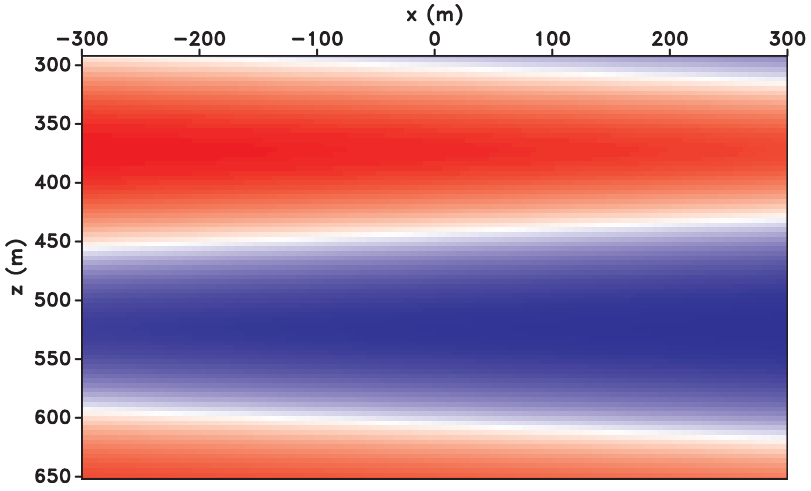
Thorbecke, J. W., and D. Draganov, 2011, Finite-difference modeling experiments for seismic interferometry: Geophysics, **76**, H1–H18.

Verschuur, D. J., A. J. Berkhout, and C. P. A. Wapenaar, 1992, Adaptive surfacerelated multiple elimination: Geophysics, **57**, 1166–1177.

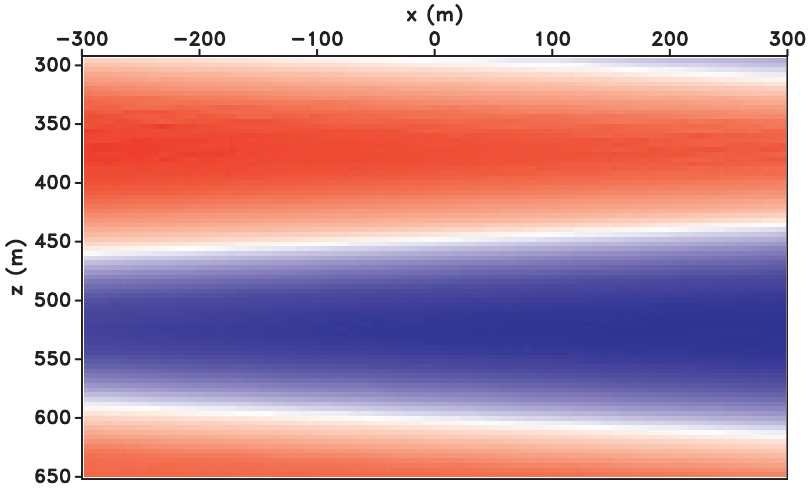
Verschuur, D. J. E., and A. J. G. Berkhout, 2011, Seismic migration of blended shot records with surface-related multiple scattering: Geophysics, **76**, A7–A13.

Wang, B., C. Mason, M. Guo, J. Cai, S. Gajawada, and D. Epili, 2010, Interactive demultiple in the postmigration depth domain: 3436–3440.

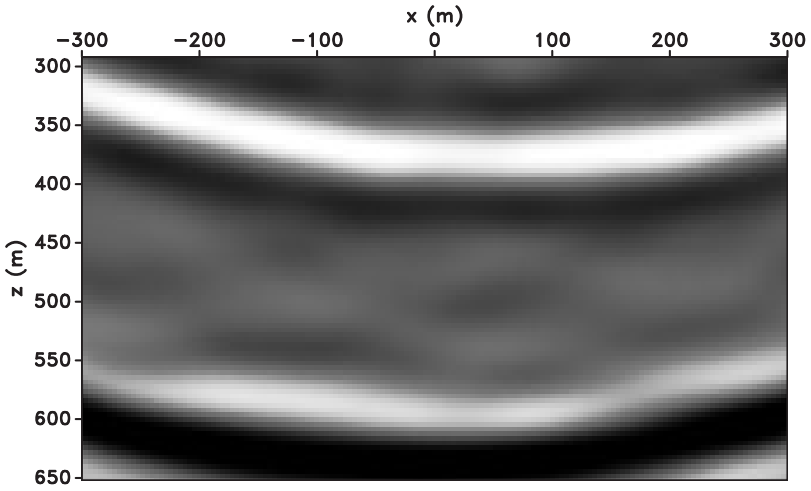
Wapenaar, K., J. Thorbecke, J. van der Neut, F. Broggini, E. Slob, and R. Snieder, 2014a, Green's function retrieval from reflection data, in absence of a receiver at the virtual source



(a)



(b)



(c)

Figure 3. Velocity retrieval: (a) is a smooth background model used for computing the transmission response T_d, (b) the retrieved velocity model, and (c) a snapshot of the wavefield $G(\mathbf{x}, \mathbf{x}_s = (0,0), t = 0.6s)$. Note how the retrieved model converges to the background model.

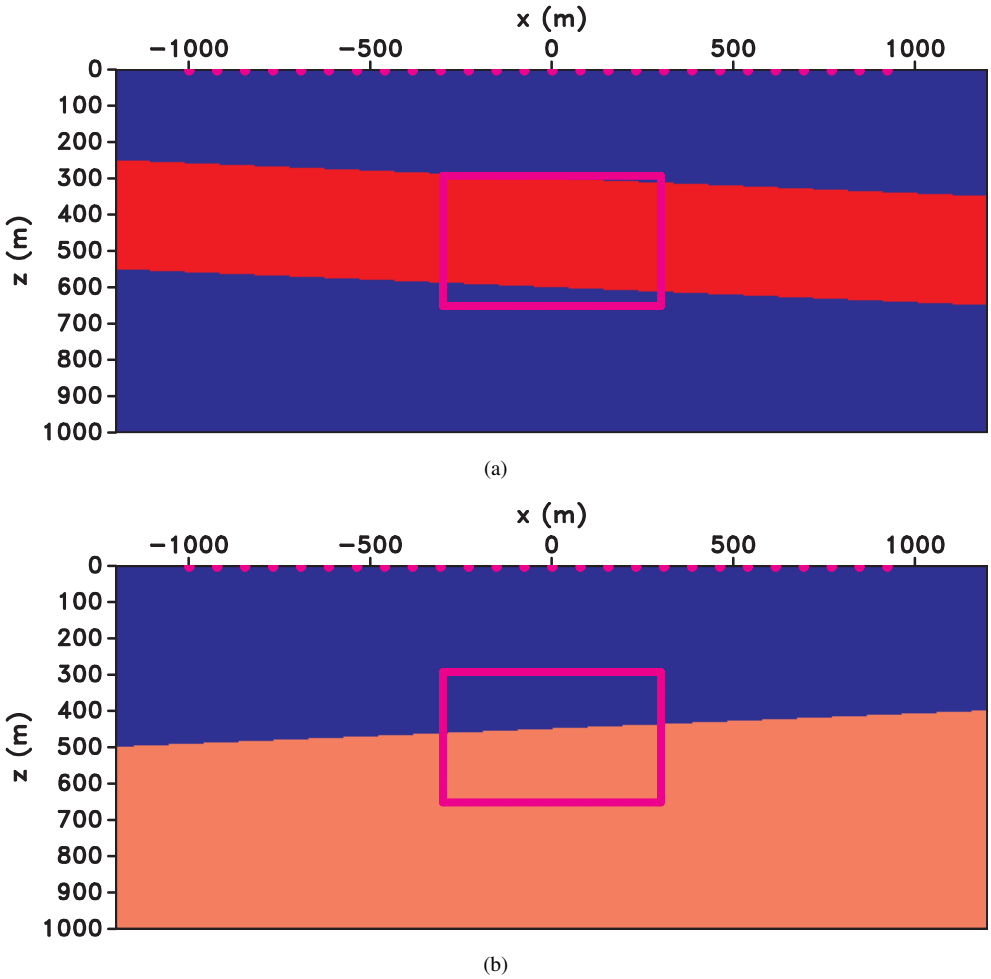


Figure 4. (a) Variable velocity and (b) density model. Note how the density and velocity model are decoupled inside the box.

position: The Journal of the Acoustical Society of America, **135**, 2847–2861.

———, 2014b, Marchenko imaging: Geophysics, **79**, WA39–WA57.

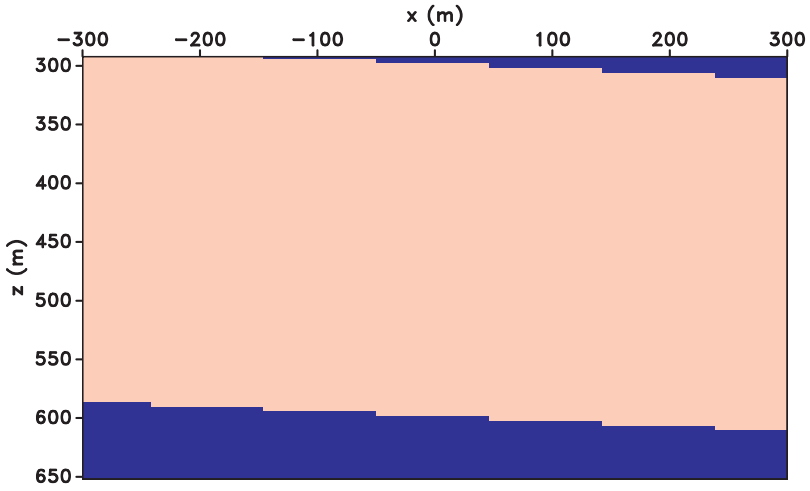
Weglein, A. B., F. A. Gasparotto, P. M. Carvalho, and R. H. Stolt, 1997, An inversescattering series method for attenuating multiples in seismic reflection data: Geophysics, **62**, 1975–1989.

Weibull, W., and B. Arntsen, 2013, Reverse time demigration using the extended imaging condition: SEG Technical Program Expanded Abstracts 2013, 4015–4020.

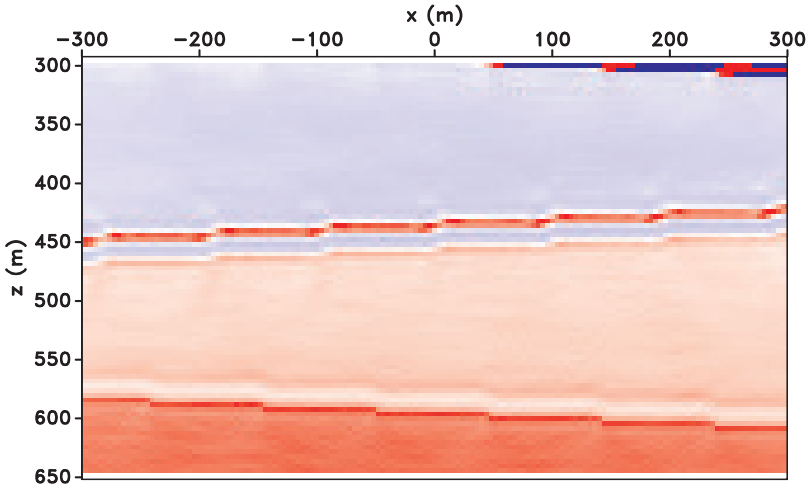
Whitmore, N. D., 1983, Iterative depth migration by backward time propagation: SEG Technical Program Expanded Abstracts, **2**, 382–385.

Whitmore, N. D., A. A. Valenciano, W. Sollner, and S. Lu, 2010, Imaging of primaries and multiples using a dualsensor towed streamer: SEG Technical Program Expanded Abstracts 2010, 3187–3192.

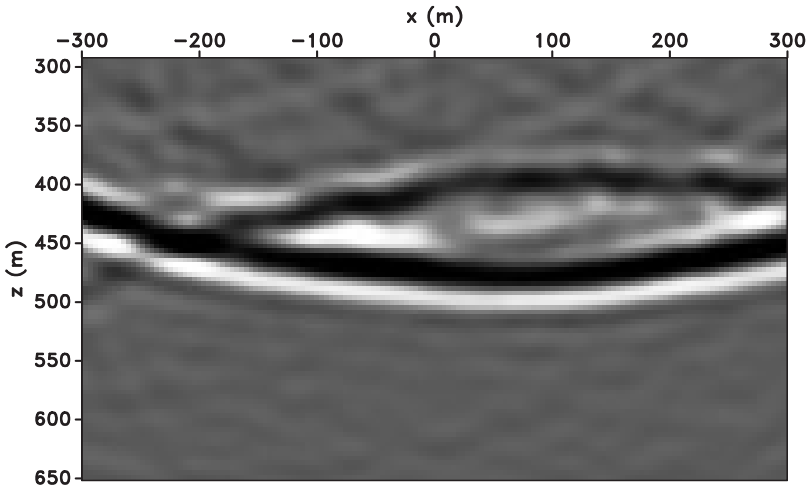
Wong, M., B. L. Biondi, and S. Ronen, 2015, Imaging with primaries and free-surface multiples by joint least-squares reverse time migration: Geophysics, **80**, S223–S235.



(a)

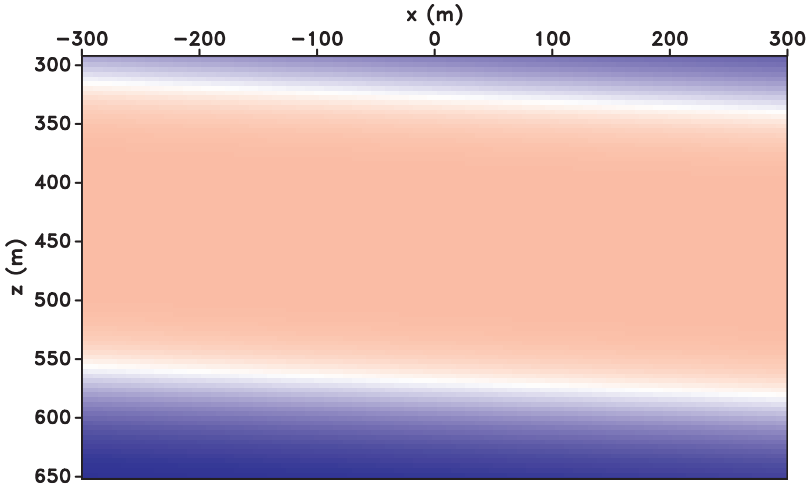


(b)

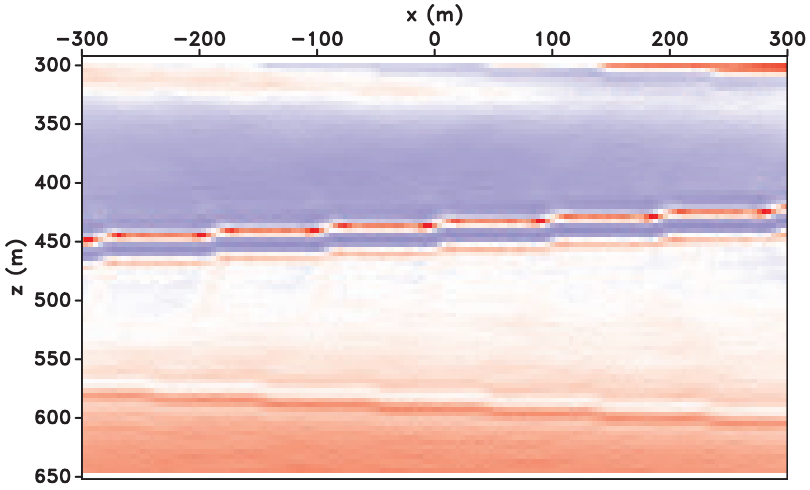


(c)

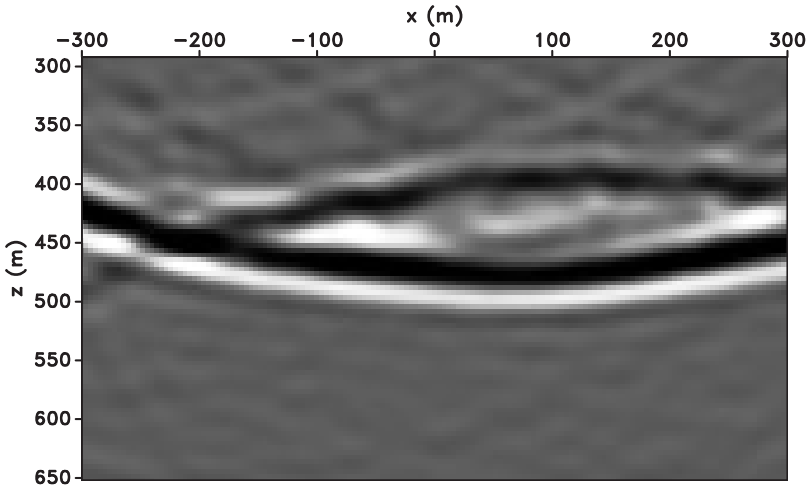
Figure 5. Density retrieval: (a) exact velocity model used as background, (b) inverted density model, and (c) a snapshot of the wavefield $G(\mathbf{x}, \mathbf{x}_s = (0,0), t = 0.6s)$. Note how the velocity layer leaks into the inverted model. However, the density layer and interface are clearly defined in the inverted model.



(a)



(b)



(c)

Figure 6. Density retrieval: (a) smooth velocity model used as background, (b) inverted density model, and (c) a snapshot of the wavefield $G(\mathbf{x}, \mathbf{x}_s = (0,0), t = 0.6s)$. Note how the velocity layer leaks into the inverted model. However, the density layer and interface are clearly defined in the inverted model.

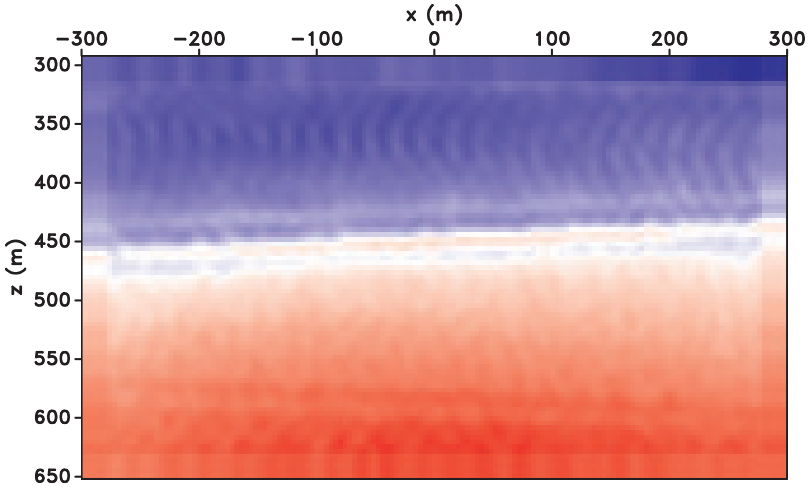


Figure 7. Density image retrieval using only the pressure wavefield in an iterative inversion process. Compare with Figure 6(b). Note how the leakage of the original velocity interfaces is attenuated.